Chapter 2
An Explanation for Why Natural Frequencies Shifting in Structures with Membrane Stresses, Using Backbone Curve Models

X. Liu, D.J. Wagg, and S.A. Neild

Abstract In this paper, the phenomenon of natural frequencies shifting due to the nonlinear stiffness effects from membrane stress is studied using a nonlinear reduced order model based on backbone curves. The structure chosen for study in this paper is a rectangular plate with a pinned constraint along all edges. To analytically explore the frequency varying phenomenon, a four nonlinear-mode based reduced-order model that contains both single-mode and coupled-mode nonlinear terms is derived. The process of deriving the reduced order model is based on a normal form transformation, combined with a Galerkin type decomposition of the governing partial differential equation of the plate. This allows a low number of ordinary differential equations to be obtained, which in turn can be used to derive backbone curves that relate directly to the nonlinear normal modes (NNMs). The frequency shifting is then investigated relative to the backbone curves. Modal interactions, caused by nonlinear terms are shown to cause the frequency shifts. In the final part of the paper, an attempt is made to quantify the frequency shifting due to different nonlinear effects.

Keywords Nonlinear reduced order model • Backbone curves • Nonlinear modal interaction • Second-order normal form method • Thin plate

2.1 Introduction

The need for accurate prediction of the nonlinear response of plates and shells has rapidly increased, especially for structures with low weight but under high environmental loads, such as aircraft fuselage structures subjected to high aeroelastic and/or acoustic loading. However, linear analysis techniques fail to capture nonlinear effects, particularly at high levels of dynamic excitation when, for example, the natural frequencies can vary with amplitude. For plate structures, it is generally accepted that when the transverse deflection approaches the thickness of the plate, the effect of the nonlinearity becomes significant. For a pinned plate, this is primarily because the in-plane stress starts to make the response amplitude dependent [1].

One approach to studying this problem is to perform full-order model simulations using a finite element software. It is often desirable to augment this approach by comparing with a reduced order modelling (ROM) or, more specifically, nonlinear reduced order modelling (NROM) techniques [2]. NROMs consist a low number of modes that include linear and nonlinear terms, typically in the form of a series of quadratic and cubic terms in the modal coordinates. The underlying linear modes can be easily determined using the classic linear modal techniques, i.e. a linear Galerkin decomposition method and linear normal form method [3]. The challenge in developing an accurate NROM is in the determination of the nonlinear stiffness coefficients. The methods for computation of the nonlinear stiffness coefficients can mainly be divided to direct and indirect approaches. The direct approaches apply the modal transformation on the full-order nonlinear stiffness matrices [4, 5] or decompose the nonlinear partial differential equations (PDE) [6]. Note this later approach is only possible for simple geomerties where a PDE model exists. The indirect approaches use static nonlinear solution of a full finite element model to determine stiffness coefficients [7–10].

Even with nonlinear reduced-order models, the forced responses can often be complex and varied which still limits the amount of design insight that can be obtained. Instead, researchers usually consider the response of the equivalent unforced and undamped systems. Many authors have studied undamped, unforced systems including beams, cables, membranes, plates

X. Liu (✉) • D.J. Wagg
Department of Mechanical Engineering, University of Sheffield, S1 3JD Sheffield, UK
e-mail: xuanang.liu@sheffield.ac.uk

S.A. Neild
Department of Mechanical Engineering, University of Bristol, Queen's Building, University Walk, BS8 1TR Bristol, UK

G. Kerschen (ed.), *Nonlinear Dynamics, Volume 1*, Conference Proceedings of the Society for Experimental Mechanics Series, DOI 10.1007/978-3-319-54404-5_2

and shells, see for example [11–13]. The free response of nonlinear systems has been studied using several different analytical approaches: nonlinear normal modes (NNMs) [14–16] and backbone curves [17–19].

In this paper we demonstrate the effect of different kinds of nonlinear stiffness terms on the natural frequency shifting behaviour by considering a rectangular plate with all edges being simply supported. In Sect. 2.2, the full-order model is built in Abaqus® and the linear and nonlinear simulation results are compared to illustrate the nonlinear dynamic behaviour of the plate under the high load excitation situation. The nonlinear reduced order model is developed by decomposing the partial differential equations of motion of the plate based on the Galerkin method in Sect. 2.3. In Sect. 2.4, the simulations results of two NROMS (uncoupled and coupled models) are quantitatively compared with the FE results. Based on the NROM, in Sect. 2.5, backbone curves of the plate obtained using the second-order normal form methods are computed to present the effects of the different nonlinear terms. Conclusions are drawn in Sect. 2.6.

2.2 Nonlinear Dynamic Behaviour of a Thin Plate

Figure 2.1 shows a schematic representation of the example plate studied in this paper with coordinate system $(O; x, y, z)$ having the origin O at one corner. For an arbitrary point of coordinates (x, y) on the middle surface of plate, its out-of-plate displacement is denoted by $w(x, y)$. All edges of the plate are simply supported and its geometric dimension and material properties are listed in Table 2.1.

Firstly, the full-order simulations were performed by Abaqus® finite element software to illustrate the resonant frequencies shifting phenomenon. 1600 thick shell elements (S8R in Abaqus) were used to discretize the plate and S8R is used as it includes membrane stretching effects for large displacements. Here the integrator, Abaqus/Implicits, in Abaqus/Standard solver was used. For ensuring a stable (physical) response, the value of the only parameter α_n specifying the integrator is chosen, $\alpha_n = -\frac{1}{6}$ to impose adequate numerical damping during integration. Each set of simulations was performed for an identical load setting with the different controls, i.e. *Nlgeom* 'Off' and 'On', for exclusion and inclusion of the nonlinear effects of large displacements respectively.

As a forcing input, random data with the sample rate of 10 kHz for a period $T = 50$ s was generated using Matlab® function *rand* initially and then substituted into Abaqus® as the random input amplitude. The model was integrated over the input period at a minimum sample time of 10^{-8} s. The displacement responses at the centre of top-right quadrant of the plate (with coordinates $[x, y] = \frac{3}{4}[a, b]$) is used as a metric, which guarantees that the contributions of the first four bending modes are included. Figure 2.2 shows the configurations of the modes considered whoses natural frequencies are $\omega_{n1} = 58.707$ rad/s, $\omega_{n2} = 143.33$ rad/s, $\omega_{n3} = 150.24$ rad/s and $\omega_{n4} = 234.83$ rad/s.

Figure 2.3 shows the response of the plate when a random uniform pressure is applied on to the left-bottom quadrant of the plate. Two different forcing magnitudes, denoted as A, were used: in Fig. 2.3a the random force magnitude is low, $A = 10^{-2}$, so that the maximum displacement response amplitude of the plate is less than 20% of the thickness of the plate, i.e. $w_{max} < 0.2h$. In Fig. 2.3b the random force magnitude is relative high, $A = 1$, so that the maximum displacement

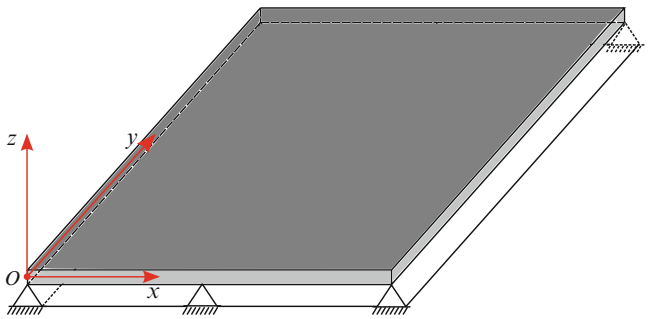

Fig. 2.1 Plate and the coordinate system

Table 2.1 Properties of the plate

Length (mm)	Width (mm)	Thickness (mm)	Density (kg/m^3)	Young's modulus (GPa)	Poisson ratio
$a = 500$	$b = 520$	$h = 5$	$\rho = 2700$	$E = 70$	$v = 0.31$

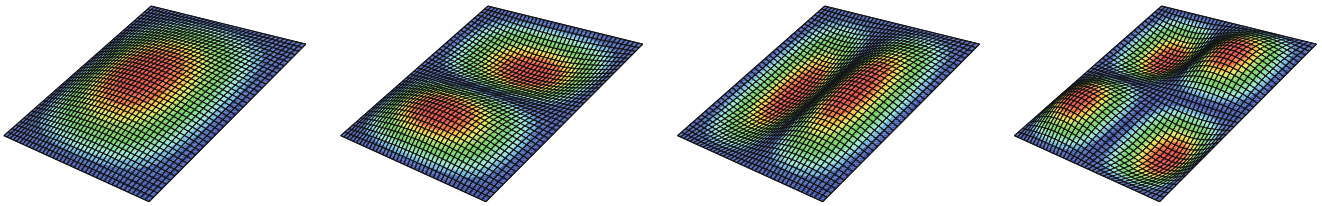

Fig. 2.2 Mode shapes of the first four bending modes of the plate

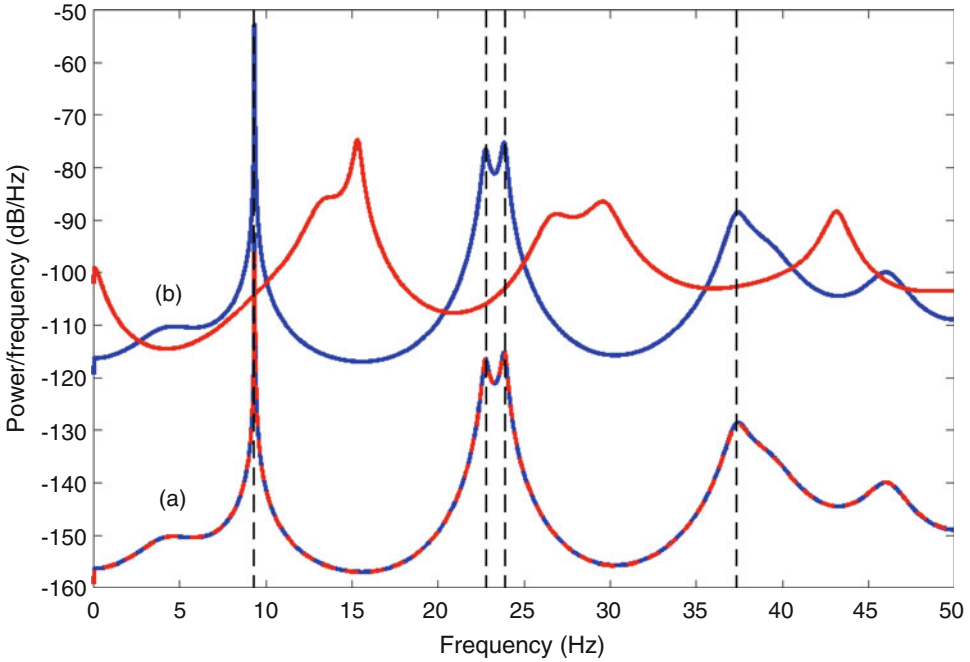

Fig. 2.3 Power spectral density of the FE simulation displacement response at the point with the coordinates $(x,\ y) = \frac{3}{4}(a,\ b)$ when the plate is under randomly excitation on left-bottom quarter area at two power level $(a)\ A = 1^{-2}$ and $(b)\ A = 1$. The *blue and red lines* represent the integration results excluding and including the nonlinear effects respectively and the *black dash lines* denote the linear modal frequencies

response amplitude is larger than the thickness of the plate, i.e. $w_{max} > h$. From Fig. 2.3, it can be seen that for the low level excitation situation the linear and nonlinear results are on top of each other and their resonant frequencies are close to the corresponding linear modal frequencies. This implies that the plate behaves linearly for this case. While when the excitation level increases, the difference between the linear and nonlinear results is obvious. For this case, the resonant frequencies of linear results are still close to the linear frequencies, but the nonlinear results have all shifted to the right significantly.

Figure 2.4 shows simulation results when the plate is under a hybrid excitation of random and harmonic forces. The random component is identical to that used for case (b) in Fig. (2.3) and the harmonic component is a point force applied at the centre of the plate. The specific sinusoidal loading point is chosen for exciting Mode I only (among the four bending modes under consideration) to increase the power (amplitude) of the first mode. Hence the frequency of the sinusoidal force is accordingly chosen to be equal to the first linear modal frequency, i.e. $\Omega = \omega_{n1}$.

From Fig. 2.3, we know that under the low level random excitation, all four modes are behaving linearly and no frequency-shifting is observed. For the linear result in Fig. 2.4, it can be seen that there is no obvious difference for the resonant frequencies and power spectral density (PSD) for Mode II, III and IV compared with Fig. 2.3 except for the PSD of Mode I increasing due to the extra harmonic force. For the nonlinear results, there are now clear double peaks around first modal frequency and furthermore the resonant frequencies are shifting to the right for Modes II, III and IV.

The results shown in Figs. 2.3 and 2.4, demonstrate how nonlinear effects can cause the resonant frequencies to shift when the amplitudes of response become large.

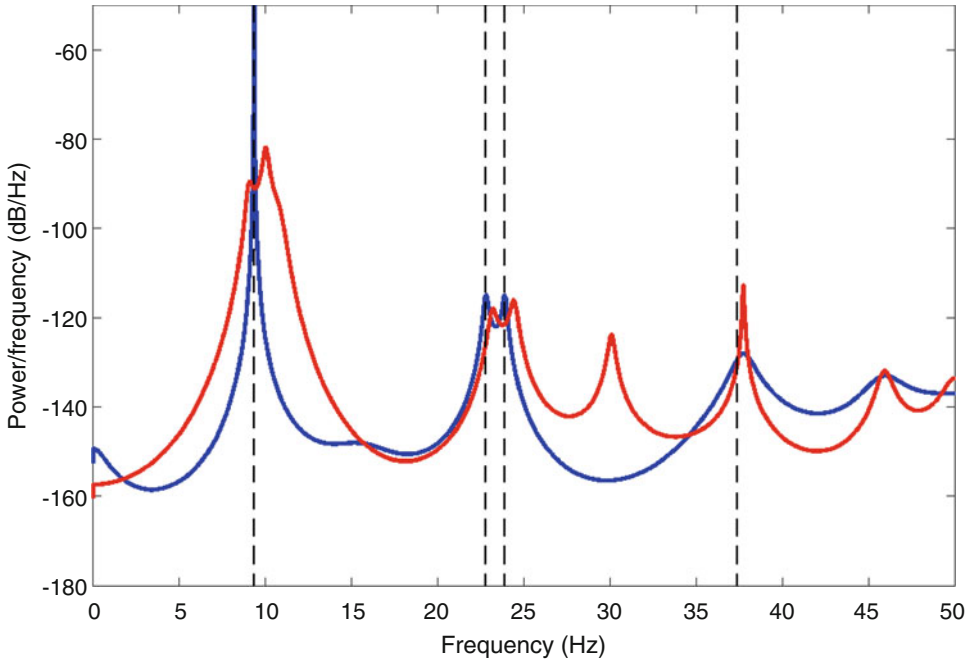

Fig. 2.4 Power spectral density of the FE simulation displacement response at the point with the coordinates $(x,\ y) = \frac{3}{4}(a,\ b)$ when the plate is under the hybrid excitation consisting of the random component identical to that used for (**a**) in Fig. 2.3 and the harmonic component with the amplitude $F_h = 5 \times 10^{-3}$ at frequency $\Omega = \omega_{n1}$

2.3 Nonlinear Reduced Order Model (NROM)

Now the nonlinear reduced order models are developed to study the nonlinear frequency shifting of the plate. The nonlinear model described in terms of modal coordinates derived by Wagg et al. [6] is used for this purpose. The derivation process of the model development is briefly introduced here and the full details can be found in [6].

Firstly, through the analysis based on the von Kármán nonlinear strain-displacement relationships, the partial differential equation of motion for the plate behaving in the nonlinear region is written as,

$$\rho h \frac{\partial^2 w}{\partial t^2} + D\nabla^2\nabla^2 w - \left(\frac{\partial^2 \Phi}{\partial y^2}\frac{\partial^2 w}{\partial x^2} - 2\frac{\partial^2 \Phi}{\partial x \partial y}\frac{\partial^2 w}{\partial x \partial y} + \frac{\partial^2 \Phi}{\partial x^2}\frac{\partial^2 w}{\partial y^2} \right) = P_f, \tag{2.1a}$$

$$\frac{1}{Eh}\nabla^2\nabla^2\Phi + \frac{\partial^2 w}{\partial x^2}\frac{\partial^2 w}{\partial y^2} - \left(\frac{\partial^2 w}{\partial x \partial y}\right)^2 = 0, \tag{2.1b}$$

where $\nabla^2 = \frac{\partial^2}{\partial x^2} + \frac{\partial^2}{\partial y^2}$, $D = \frac{Eh^3}{12[1-v^2]}$ and other parameters are defined in [6]. Substituting the Galerkin variables,

$$w(x, y, t) = \sum_{1}^{M}\sum_{1}^{N} X_m(x) Y_n(y) q_{mn}(t), \tag{2.2}$$

and the Airy function

$$\Phi(x, y, t) = \sum_{1}^{R}\sum_{1}^{S} \Theta_r(x) \Psi_s(y) F_{rs}(t), \tag{2.3}$$

into Eq. (2.1), where $q_{mn}(t)$ is a time-dependent modal coordinate and $X_n(x)$ and $Y_m(y)$ are the mode shapes, and then applying the orthogonality conditions gives a set of ordinary differential equations of motion of vibration modes as

$$\ddot{q}_{\mathrm{ij}} + \omega_{\mathrm{ij}}^2 q_{\mathrm{ij}} + \sum^{\mathrm{M,N,G,H,T,U,R,S}} \frac{\Gamma_{1\mathrm{ghturs}}\Gamma_{3\mathrm{mnrsij}}}{\Gamma_{2\mathrm{rs}}} q_{\mathrm{gh}} q_{\mathrm{tu}} q_{\mathrm{mn}} = f_{ij}. \tag{2.4}$$

where,

$$\omega_{\mathrm{ij}}^2 = \pi^2 \left(\frac{i^2}{a^2} + \frac{j^2}{b^2}\right)\sqrt{\frac{D}{\rho h}}, \qquad f_{\mathrm{ij}} = \int_0^a \int_0^b P_f X_{\mathrm{i}} Y_{\mathrm{j}} \mathrm{d}y\mathrm{d}x, \tag{2.5}$$

and,

$$\Gamma_{1\mathrm{ghturs}} = \int_0^a \int_0^b \left(\frac{\mathrm{d}^2 X_{\mathrm{g}}}{\mathrm{d}x^2} Y_{\mathrm{h}} X_{\mathrm{t}} \frac{\mathrm{d}^2 Y_{\mathrm{u}}}{\mathrm{d}y^2} - \left(\frac{\mathrm{d}X_{\mathrm{g}}}{\mathrm{d}x}\frac{\mathrm{d}Y_{\mathrm{h}}}{\mathrm{d}y}\frac{\mathrm{d}X_{\mathrm{t}}}{\mathrm{d}x}\frac{\mathrm{d}Y_{\mathrm{u}}}{\mathrm{d}y}\right)\right)\Theta_{\mathrm{r}}\Psi_{\mathrm{s}}\mathrm{d}y\mathrm{d}x, \tag{2.6a}$$

$$\Gamma_{2\mathrm{rs}} = \frac{ab}{4Eh}\pi^4 \left(\frac{r^2}{a^2} + \frac{s^2}{b^2}\right)^2, \tag{2.6b}$$

$$\begin{aligned}\Gamma_{3\mathrm{mnrsij}} = &\frac{4}{\rho h a b}\int_0^a \int_0^b \Big(\Theta_{\mathrm{r}} \frac{\mathrm{d}^2\Psi_{\mathrm{s}}}{\mathrm{d}y^2}\frac{\mathrm{d}^2 X_{\mathrm{m}}}{\mathrm{d}x^2} Y_{\mathrm{n}} \\ &- 2\frac{\mathrm{d}\Theta_{\mathrm{r}}}{\mathrm{d}x}\frac{\mathrm{d}\Psi_{\mathrm{s}}}{\mathrm{d}y}\frac{\mathrm{d}X_{\mathrm{n}}}{\mathrm{d}x}\frac{\mathrm{d}Y_{\mathrm{m}}}{\mathrm{d}y} + \frac{\mathrm{d}^2\Theta_{\mathrm{r}}}{\mathrm{d}x^2}\Psi_{\mathrm{s}} X_{\mathrm{m}}\frac{\mathrm{d}^2 Y_{\mathrm{n}}}{\mathrm{d}y^2}\Big) X_{\mathrm{i}} Y_{\mathrm{j}}\mathrm{d}y\mathrm{d}x.\end{aligned} \tag{2.6c}$$

For the plate with a simply supported boundary condition, the mode shapes and space functions of the Airy functions are,

$$X_{\mathrm{m}}(x) = \sin\left(\frac{m\pi}{a}x\right),\ Y_{\mathrm{n}}(y) = \sin\left(\frac{n\pi}{b}y\right),\ \Theta_{\mathrm{r}}(x) = \sin\left(\frac{r\pi}{a}x\right),\ \Psi_{\mathrm{s}}(y) = \sin\left(\frac{s\pi}{b}y\right). \tag{2.7}$$

Substituting Eq. (2.7) with the parameters values of the plate in Table 2.1 into Eqs. (2.4)–(2.6) with the imposed modal damping terms gives equations of motion in the modal coordinates that can be written as

$$\ddot{\mathbf{q}} + \mathbf{C}\mathbf{q} + \mathbf{\Lambda}\mathbf{q} + \mathbf{N}_q(\mathbf{q}) = \mathbf{F}_m, \tag{2.8}$$

where $\mathbf{C}$ is a vector of damping coefficients, $\mathbf{\Lambda}$ is a diagonal matrix of the squares of modal natural frequencies, $\mathbf{N}_q$ is the column vector containing the nonlinear terms whose lth element may be written

$$N_q^{(l)} = \sum_{r=1}^{N}\sum_{s=r}^{N}\sum_{t=s}^{N} \alpha_n^{(l)} q_r q_s q_t, \tag{2.9}$$

and $\mathbf{F}_m$ is a vector of modal forcing terms. Table 2.2 lists the values of the linear modal natural frequencies and the non-zero coefficients of nonlinear terms for the first four modes of the plate.

2.4 Simulation Results of the NROM

From Eq. (2.9), we know that there exist two types of nonlinear terms, i.e. single-mode nonlinear terms, q_i^3, and coupled-mode nonlinear terms, $q_i q_j q_k$ (where $i \neq j$ and $i \neq k$) in the equation of motion of ith mode. In order to study the effect of the nonlinear terms on resonant frequency shift, two kinds of nonlinear four-mode truncation models for the example structure are used, i.e. the coupled (with nonlinear coupled-mode terms) and uncoupled (no coupled-mode terms) cases. Their respective equations of motion are stated as,

$$\ddot{\mathbf{q}} + \mathbf{C}\dot{\mathbf{q}} + \Lambda\mathbf{q} + \mathbf{N}_q(\mathbf{q}) = \mathbf{F}_m(t) \quad \text{and} \quad \ddot{\tilde{\mathbf{q}}} + \mathbf{C}\dot{\tilde{\mathbf{q}}} + \Lambda\tilde{\mathbf{q}} + \tilde{\mathbf{N}}_{\tilde{q}}(\tilde{\mathbf{q}}) = \mathbf{P}_m(t), \tag{2.10}$$

Table 2.2 Model coefficients for the lowest four nonlinear modes of the plate

Mode no.	ω_n (rad/s)	Coefficients ($\times 10^9$)	Nonlinear term
I	58.9	$\alpha_1^I = 5.45$	q_1^3
		$\alpha_2^I = 23.6$	$q_1 q_2^2$
$i = 1, j = 1$		$\alpha_3^I = 22.7$	$q_1 q_3^2$
		$\alpha_4^I = 24.4$	$q_1 q_4^2$
		$\alpha_5^I = 74.3$	$q_2 q_3 q_4$
II	143.9	$\alpha_1^{II} = 23.6$	$q_1^2 q_2$
		$\alpha_2^{II} = 31.4$	q_2^3
$i = 1, j = 2$		$\alpha_3^{II} = 65.1$	$q_2 q_3^2$
		$\alpha_4^{II} = 124.3$	$q_2 q_4^2$
		$\alpha_5^{II} = 74.3$	$q_1 q_3 q_4$
III	150.8	$\alpha_1^{III} = 22.7$	$q_1^2 q_3$
		$\alpha_2^{III} = 65.1$	$q_2^2 q_3$
$i = 2, j = 1$		$\alpha_3^{III} = 31.4$	q_3^3
		$\alpha_4^{III} = 132.4$	$q_3 q_4^2$
		$\alpha_5^{III} = 74.3$	$q_1 q_2 q_4$
IV	235.8	$\alpha_1^{IV} = 24.4$	$q_1^2 q_4$
		$\alpha_2^{IV} = 124.3$	$q_2^2 q_4$
$i = 2, j = 2$		$\alpha_3^{IV} = 132.4$	$q_3^2 q_4$
		$\alpha_4^{IV} = 55.8$	q_4^3
		$\alpha_5^{IV} = 74.3$	$q_1 q_2 q_3$

where the modal force vector $\mathbf{F}_m(t)$ may be written

$$\mathbf{F}_m = \mathbf{P}_r r(t) + \mathbf{P}_h \cos(\Omega t), \tag{2.11}$$

where $r(t)$ is the random input signal, $\mathbf{P}_r$ is the vector magnitude of the modal random force component and $\mathbf{P}_h$ is the vector amplitude of the harmonic component. $\mathbf{N}_q$ and $\tilde{\mathbf{N}}_{\tilde{q}}$ are the nonlinear term vectors, written

$$\mathbf{N}_q = \begin{pmatrix} \alpha_1^I q_1^3 + \alpha_2^I q_1 q_2^2 + \alpha_3^I q_1 q_3^2 + \alpha_4^I q_1 q_4^2 + \alpha_5^I q_2 q_3 q_4 \\ \alpha_1^{II} q_1^2 q_2 + \alpha_2^{II} q_2^3 + \alpha_3^{II} q_2 q_3^2 + \alpha_4^{II} q_2 q_3^2 + \alpha_5^{II} q_1 q_3 q_4 \\ \alpha_1^{III} q_1^2 q_3 + \alpha_2^{III} q_2^2 q_3 + \alpha_3^{III} q_3^3 + \alpha_4^{III} q_3 q_4^2 + \alpha_5^{III} q_1 q_2 q_4 \\ \alpha_1^{IV} q_1^2 q_4 + \alpha_2^{IV} q_2^2 q_4 + \alpha_3^{IV} q_3^2 q_4 + \alpha_4^{IV} q_4^3 + \alpha_5^{IV} q_1 q_2 q_3 \end{pmatrix}, \text{ and } \tilde{\mathbf{N}}_{\tilde{q}} = \begin{pmatrix} \alpha_1^I \tilde{q}_1^3 \\ \alpha_2^{II} \tilde{q}_2^3 \\ \alpha_3^{III} \tilde{q}_3^3 \\ \alpha_4^{IV} \tilde{q}_4^3 \end{pmatrix}. \tag{2.12}$$

In both NROMs, the viscous damping is used and the damping ratio is $\zeta = 0.1\%$ for all modes. These two equations are integrated over the identical force time history defined at discrete data points using the fourth order Runge-Kutta integration operator. The random data used is identical to that used in the previous FE simulation. The discrete time period between consecutive time history points is 10^{-4} s and the integration was performed over a time period of 50 s. The displacement response at the identical point considered in the FE simulation is here used again.

Figure 2.5 shows the simulation results of Eq. (2.10) when $\mathbf{P}_r = \frac{4\times 10^{-2}}{\pi^2 \rho h}[1,\ 1,\ 1,\ 1]^{\mathrm{T}}$ and $\mathbf{P}_r = \frac{4}{\pi^2 \rho h}[1,\ 1,\ 1,\ 1]^{\mathrm{T}}$ with $\mathbf{P}_h = [0,\ 0,\ 0,\ 0]^{\mathrm{T}}$ which is equivalent to the excitation situation used for FE results in Fig. 2.3, i.e. $P_f(x, y) = r(t)$ and $P_f(x, y) = 10r(t)$ for $0 \le x \le \frac{1}{2}a, 0 \le y \le \frac{1}{2}b$. From the results when $\mathbf{P}_r = \frac{4\times 10^{-2}}{\pi^2 \rho h}[1,\ 1,\ 1,\ 1]^{\mathrm{T}}$, it can be seen that the results of uncoupled and coupled models are nearly identical and their resonant frequencies are close to the linear modal frequencies. As expected, this confirms that the effect of the modal coupling terms is insignificant for the low response amplitude situation. For the high-level excitation situation, the resonant frequencies for both models have shifted to higher frequencies. However the frequency shift level of the coupled model is more obvious than that of the uncoupled model.

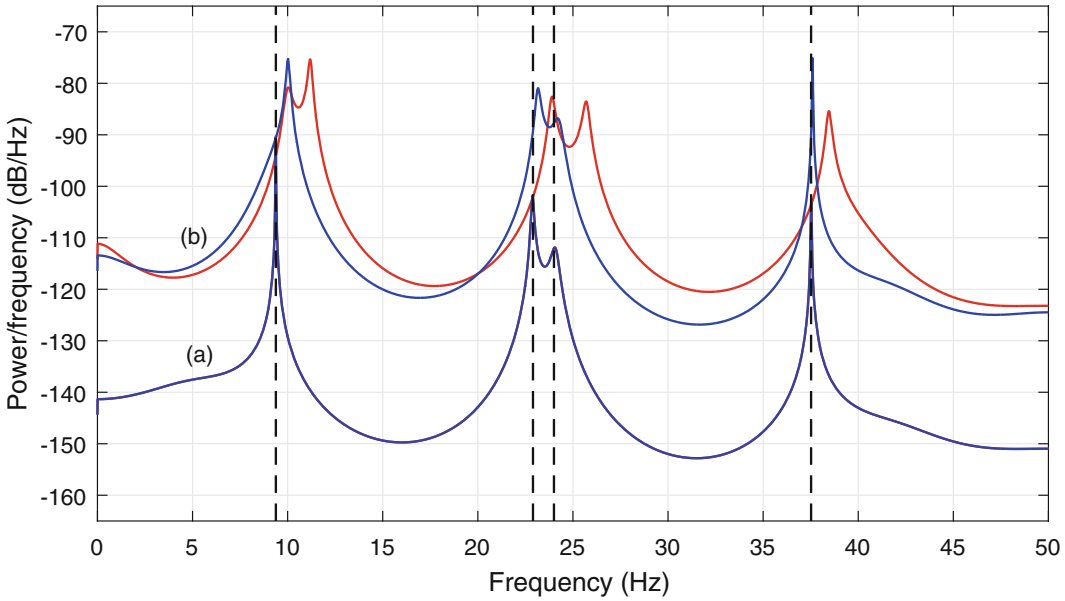

Fig. 2.5 Power spectral density of the NROM simulation displacement response $x = q_1 + \frac{\sqrt{2}}{2}q_2 + \frac{\sqrt{2}}{2}q_3 + \frac{1}{2}q_4$ which is equivalent to that of the point with the coordinates $(x,\ y) = \frac{3}{4}(a,\ b)$ at the plate when all four modes are randomly excited at two different power levels: (**a**) $\mathbf{P}_r = \frac{4\times10^{-2}}{\pi^2\rho h}[1,\ 1,\ 1,\ 1]^{\mathrm{T}}$. (**b**) $\mathbf{P}_r = \frac{4}{\pi^2\rho h}[10,\ 10,\ 10,\ 10]^{\mathrm{T}}$. The *blue and red lines* represent the results of the uncoupled and coupled models respectively and the *black lines* denote the linear modal frequencies

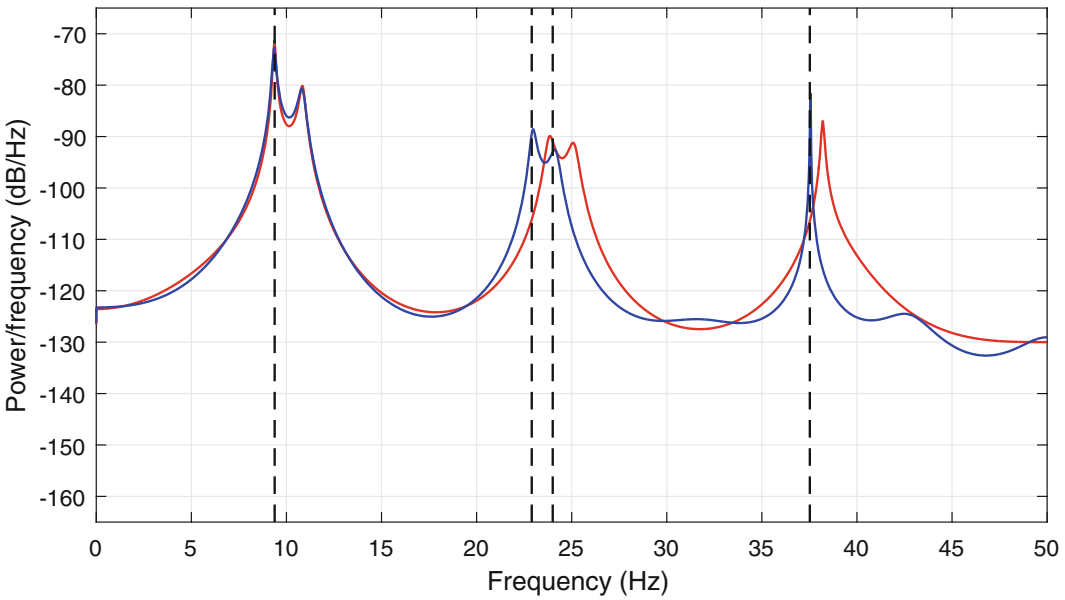

Fig. 2.6 Power spectral density of the NROM simulation displacement response $x = q_1 + \frac{\sqrt{2}}{2}q_2 + \frac{\sqrt{2}}{2}q_3 + \frac{1}{2}q_4$ which is equivalent to that of the point with the coordinates $(x,\ y) = \frac{3}{4}(a,\ b)$ when all four modes are randomly excited and Mode *I* is sinusoidal forced simultaneously: $\mathbf{P}_r = \frac{4\times10^{-1}}{\pi^2\rho h}[1,\ 1,\ 1,\ 1]^{\mathrm{T}}$, $\mathbf{P}_h = \frac{4\times10^{-3}}{\rho hab}[5,\ 0,\ 0,\ 0]^{\mathrm{T}}$ and $\Omega = \omega_{n1}$

This implies that both single-mode terms and coupled-terms can cause frequency shifting in the nonlinear region. For this case, both models are regarded to be qualitatively correct compared with the full-order simulation results.

Furthermore, the NROM is used to simulate the plate under excitation situation considered in Fig. 2.4, so the force amplitude $\mathbf{P}_r = \frac{4\times10^{-1}}{\pi^2\rho h}[1,\ 1,\ 1,\ 1]^{\mathrm{T}}$ and $\mathbf{P}_h = \frac{4\times10^{-3}}{\rho hab}[5,\ 0,\ 0,\ 0]^{\mathrm{T}}$ was used and the results are presented in Fig. 2.6. We can see that for Modes *II*, *III* and *IV*, the resonant frequencies of the coupled model have a frequency shift, while the

uncoupled model results do not compared with the linear modal frequencies. For this case, it is the coupled model that can more accurately represent the nonlinear behaviour of the full-order FE model.

2.5 Effect of the Nonlinear Coupled-Mode Terms Explanation

In this section, we use the backbone curves to illustrate the effect of the nonlinear terms on the frequency shifting. The backbone curves describe the loci of dynamic responses of a system unforced and undamped and can be used to represent the global dynamic characteristics of the system. In order to compute backbone curves, the second-order normal form technique is applied to solve the nonlinear equation of motion of the plate. This technique consists of a series of transformations which result in approximated expressions for the resonant modal equation of motion describing the dynamics of the fundamental response components of the nonlinear system. These expressions can be solved to find the relationship between the fundamental responses amplitude and frequency of the underlying linear modes which can then be used, along with the inverse of the aforementioned transformation, to find the harmonic components and the responses in the physical coordinates.

Here, only the outcome of the application of this technique to the example system is given and the complete description related to the second-order normal form method can be found in [6].

From Eq. (2.8), the equation of motion for the equivalent conservative system is written

$$\ddot{\mathbf{q}} + \mathbf{\Lambda}\mathbf{q} + \mathbf{N}_{\mathrm{q}}(\mathbf{q}) = \mathbf{0}, \tag{2.13}$$

which, after the application of the second-order normal form method, results in the time-invariant equations, such that

$$\left[\left(\omega_{n1}^2 - \omega_{r1}^2\right) + \frac{1}{4}\left(3\alpha_1^I U_1^2 + 2\alpha_2^I U_2^2 + 2\alpha_3^I U_3^2 + 2\alpha_4^I U_4^2\right)\right] U_1 = 0, \tag{2.14a}$$

$$\left[\left(\omega_{n2}^2 - \omega_{r2}^2\right) + \frac{1}{4}\left(2\alpha_1^{II} U_1^2 + 3\alpha_2^{II} U_2^2 + (2+p)\alpha_3^{II} U_3^2 + 2\alpha_4^{II} U_4^2\right)\right] U_2 = 0, \tag{2.14b}$$

$$\left[\left(\omega_{n3}^2 - \omega_{r3}^2\right) + \frac{1}{4}\left(2\alpha_1^{III} U_1^2 + (2+p)\alpha_2^{III} U_2^2 + 3\alpha_3^{III} U_3^2 + 2\alpha_4^{IV}\right)\right] U_3 = 0, \tag{2.14c}$$

$$\left[\left(\omega_{n4}^2 - \omega_{r4}^2\right) + \frac{1}{4}\left(2\alpha_1^{IV} U_1^2 + 2\alpha_2^{IV} U_2^2 + 2\alpha_3^{IV} U_3^2 + 3\alpha_4^{IV} U_4^2\right)\right] U_4 = 0, \tag{2.14d}$$

where $p = \mathrm{e}^{\mathrm{j}2|\phi_2 - \phi_3|}$ and U_i, ω_{ri} and ϕ_i are the fundamental response amplitude, frequency and phase of q_i respectively. Through successively setting $U_2 = U_3 = U_4 = 0$, $U_1 = U_3 = U_4 = 0$, $U_1 = U_2 = U_4 = 0$ and $U_1 = U_2 = U_3 = 0$ in Eq. (2.14) we obtain the expressions of four single-mode backbones, as

$$S_1: \qquad \omega_{r1}^2 = \omega_{n1}^2 + \frac{3}{4}\alpha_1^I U_1^2, \tag{2.15a}$$

$$S_2: \qquad \omega_{r2}^2 = \omega_{n2}^2 + \frac{3}{4}\alpha_2^{II} U_2^2, \tag{2.15b}$$

$$S_3: \qquad \omega_{r3}^2 = \omega_{n3}^2 + \frac{3}{4}\alpha_3^{III} U_3^2. \tag{2.15c}$$

$$S_4: \qquad \omega_{r4}^2 = \omega_{n4}^2 + \frac{3}{4}\alpha_4^{IV} U_4^2. \tag{2.15d}$$

In addition, there exist two in-unison double-mode backbone curves $D_{23(i)}^{+}$ and $D_{23(i)}^{-}$ composed of contributions of Mode *II* and *III* which can be calculated by using an identical expression,

$$D_{23(i)}^{\pm}: \begin{cases} U_3^2 = U_{(i)}^2 + \eta_{(i)} U_2^2, \\ \Omega^2 = \omega_{(i)}^2 + \frac{3}{4}\gamma_{(i)} U_2^2. \end{cases} \tag{2.16}$$

where, $U_{(i)}$, $\omega_{(i)}$, $\eta_{(i)}$ and $\gamma_{(i)}$ are time-invariant that

$$U_{(i)}^2 = \frac{4}{3}\frac{\omega_{n3}^2 - \omega_{n2}^2}{\alpha_3^{II} - \alpha_3^{III}},\ \omega_{(i)} = \frac{\alpha_3^{II}\omega_{n3}^2 - \alpha_3^{III}\omega_{n2}^2}{\alpha_3^{II} - \alpha_3^{III}},\ \eta_{(i)} = \frac{\alpha_2^{III} - \alpha_2^{II}}{\alpha_3^{II} - \alpha_3^{III}},\ \gamma_{(i)} = \frac{\alpha_3^{II}\alpha_2^{III} - \alpha_2^{II}\alpha_3^{III}}{\alpha_3^{II} - \alpha_3^{III}}. \tag{2.17}$$

For backbone curves $D_{23(i)}^{+}$, the modal coordinates are in-phase while for $D_{23(i)}^{-}$ the modes are anti-phase, i.e.

$$D_{23(i)}^{+} : |\phi_2 - \phi_3| = 0, \qquad D_{23(i)}^{-} : |\phi_2 - \phi_3| = \pi. \tag{2.18}$$

As for the above backbone curves, their expressions are based on the assumption that any other non-resonant coupled mode, is not activated.

Now, if the Mode *I* and *IV* are assumed to be activated and respond sinusoidally at any frequencies except for those that may potentially cause resonant interaction with Mode *II* or *III*, such as $\omega_{r1(4)} = \frac{1}{3}\omega_{r2(3)}$ or $\omega_{r1(4)} = \omega_{r2(3)}$, the expressions of backbone curves for Mode *II* and *III* are modified. For the single-mode backbone curves which are noted as $\hat{S}_2$ and $\hat{S}_3$ for distinction, they can be calculated using,

$$\hat{S}_2 : \qquad \omega_{r2}^2 = \hat{\omega}_{n2}^2 + \frac{3}{4}\alpha_2^{II}U_2^2, \tag{2.19}$$

$$\hat{S}_3 : \qquad \omega_{r3}^2 = \hat{\omega}_{n3}^2 + \frac{3}{4}\alpha_3^{III}U_3^2, \tag{2.20}$$

where

$$\hat{\omega}_{n2} = \omega_{n2}^2 + \frac{1}{2}\left(\alpha_1^{II}U_1^2 + \alpha_4^{II}U_4^2\right) \quad \text{and} \quad \hat{\omega}_{n3} = \omega_{n3}^2 + \frac{1}{2}\left(\alpha_1^{III}U_1^2 + \alpha_4^{III}U_4^2\right). \tag{2.21}$$

For the double-mode backbone curves, $\hat{D}_{23(i)}^{\pm}$, their expressions are changed to be

$$\hat{D}_{23(i)}^{\pm} : \begin{cases} U_3^2 = \hat{U}_{s_3(i)}^2 + \eta_{s_3(i)}U_2^2, \\ \Omega^2 = \hat{\omega}_{s_3(i)}^2 + \frac{3}{4}\gamma_{s_3(i)}U_2^2. \end{cases} \tag{2.22}$$

where,

$$\hat{U}_{(i)}^2 = U_{(i)}^2 + \mu_{1(i)}U_1^2 + \mu_{4(i)}U_4^2 \quad \text{and} \quad \hat{\omega}_{(i)}^2 = \omega_{(i)}^2 + \frac{1}{2}\left(\nu_{1(i)}U_1^2 + \nu_{4(i)}U_4^2\right). \tag{2.23}$$

Here the constants $\mu_{1(i)}$, $\mu_{4(i)}$, $\nu_{1(i)}$ and $\nu_{4(i)}$ are computed using

$$\mu_{1(i)} = \frac{2}{3}\frac{\alpha_1^{III} - \alpha_1^{II}}{\alpha_3^{II} - \alpha_3^{III}},\ \mu_{4(i)} = \frac{2}{3}\frac{\alpha_4^{III} - \alpha_4^{II}}{\alpha_3^{II} - \alpha_3^{III}},\ \nu_{1(i)} = \frac{\alpha_3^{II}\alpha_1^{III} - \alpha_1^{II}\alpha_3^{III}}{\alpha_3^{II} - \alpha_3^{III}},\ \nu_{4(i)} = \frac{\alpha_3^{II}\alpha_4^{III} - \alpha_4^{II}\alpha_3^{III}}{\alpha_3^{II} - \alpha_3^{III}}. \tag{2.24}$$

Comparing Eqs. (2.15b), (2.15c) and (2.16) with Eqs. (2.19), (2.20) and (2.22), the general computation expressions of backbone curves are identical for the situation with and without the effect of Mode *I* and *IV*. While, considering Eqs. (2.21) and (2.23), it can be seen that by considering the non-resonant modes the resonant frequencies of both single- and double-backbone curves of Mode *II* and *III* increase or decrease depending on the sign of the corresponding coefficients and the frequency varying level depends on the values of the response amplitude of Mode *I* and *IV*.

Figure 2.7 shows backbone curves results of Mode *II* and *III* of the example plate. Note that the coordinates are nondimentionalised using $\bar{U}_i = U_i/h$ and $\bar{\Omega} = \Omega/\omega_{n2}$ and $U_4 = 0$ is used otherwise the results cannot be presented visually. In Fig. 2.7, the backbone curves have been projected onto a three-dimensional space of the modal response amplitude against frequency with varying response amplitude of Mode *I*. From the results, it can be seen that the resonant response frequencies of all backbone curves for Mode *II* and *III* have shifted to higher frequency-increasing as $\bar{U}_1$ increases.

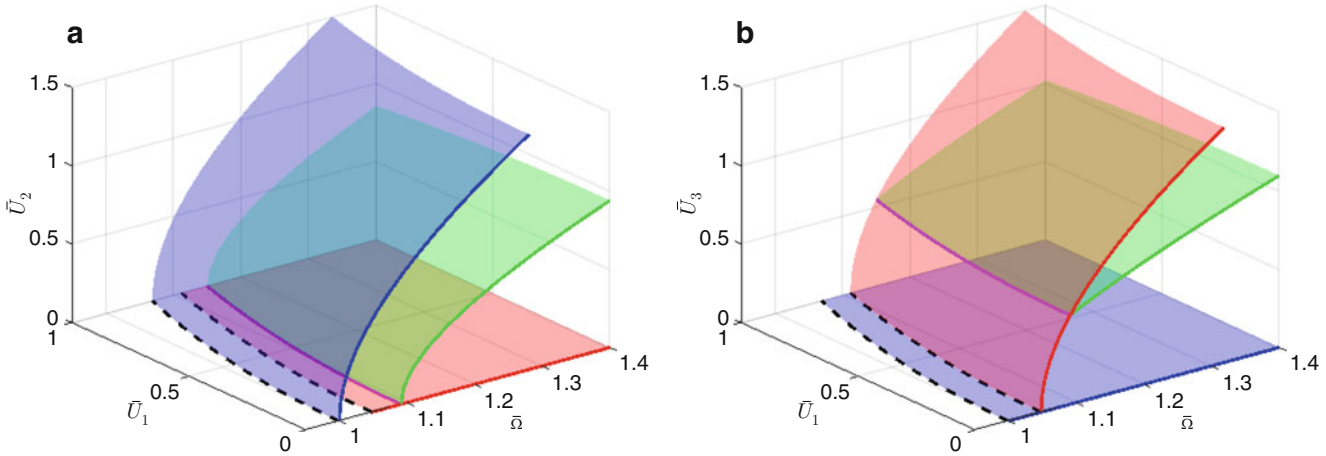

Fig. 2.7 Backbone curves of nonlinear normal modes *II*, in **(a)**, and *III*, in **(b)**, of the example plate with varying response amplitude of mode *I*. Single-mode backbone curves $\hat{S}_2$ and $\hat{S}_3$ are shaded in *blue and red* respectively and double-mode backbone curves, $\hat{D}^{\pm}_{23(i)}$ are in *green*. The *black dash lines* indicate the effective linear natural frequencies described by Eq. (2.21) and *magenta lines* indicate the effective bifurcation points described by Eq. (2.23). *Blue, red and green lines* represent the backbone curves S_2, S_3 and $D^{\pm}_{23(i)}$ respectively

2.6 Conclusions

In this paper, the nonlinear dynamic behaviour of a rectangular plate with an ideal edge-pinned constrain has been considered. In particular, the effects of different nonlinear terms, i.e. single-mode and coupled-mode terms, on the natural frequency shifting have been analysed. This is an important topic because it may be helpful for selection of nonlinear terms included in nonlinear reduced order models for different excitation situations.

First, we modelled the plate in the finite element software, Abaqus®, and the implicit integrator in Abaqus/Standard was used for integrating the response for two cases of force configuration, i.e. random and hybrid excitation. The results including and excluding the effect of geometrical nonlinearity were compared to show the nonlinear effect on the natural frequency. Then the partial differential equation of motion of the plate was used to directly compute the nonlinear reduced order model. Based on the 'full' nonlinear reduced order model, two kinds of four-mode truncation models, i.e. coupled and uncoupled models, for the example plate were used for response simulation. The results were compared with the nonlinear behaviour predicted by the full FE model.

Finally, the second-order normal form method was used to estimate the backbone curves including the nonlinear modal interactions. From the results, we can see that for the low response situation, the effect of all nonlinear terms is insignificant which is consistent to the finding in the existing literature. When the nonlinear systems under a high loading, nonlinear cross-coupling terms are the main mechanism that cause frequency shifting for the multi-mode excitation situations. This findings in this paper may be useful for the nonlinear terms selection in nonlinear reduced order models that are significant for nonlinear system response prediction and identification.

References

1. Chia, C.-Y.: Nonlinear Analysis of Plates. McGraw-Hill, New York (1980)
2. Mignolet, M.P., Przekop, A., Rizzi, S.A., Spottswood, S.M.: A review of indirect/non-intrusive reduced order modeling of nonlinear geometric structures. J. Sound Vib. **332**(10), 2437–2460 (2013)
3. Nayfeh, A.H., Mook, D.T.: Nonlinear Oscillations. Wiley, New York (2008)
4. Nash, M.: Nonlinear structural dynamics by finite element model synthesis. PhD thesis, Imperial College London, University of London (1978)
5. Shi, Y., Mei, C.: A finite element time domain modal formulation for large amplitude free vibrations of beams and plates. J. Sound Vib. **193**(2), 453–464 (1996)
6. Wagg, D., Neild, S.: Nonlinear Vibration with Control: For Flexible and Adaptive Structures. Springer, Berlin (2014)
7. Muravyov, A.A., Rizzi, S.A.: Determination of nonlinear stiffness with application to random vibration of geometrically nonlinear structures. Commun. Strateg. **81**(15), 1513–1523 (2003)
8. McEwan, M.I., Wright, J.R., Cooper, J.E., Leung, A.Y.T.: A finite element/modal technique for nonlinear plate and stiffened panel response prediction. In: Proceedings of the 42nd AIAA/ASME/ASCE/AHS/ASC Structures, Structural Dynamics, and Materials Conference and Exhibit Technical Papers, pp. 3061–3070 (2001)

9. McEwan, M.I., Wright, J.R., Cooper, J.E., Leung, A.Y.T.: A combined modal/finite element analysis technique for the dynamic response of a non-linear beam to harmonic excitation. J. Sound Vib. **243**(4), 601–624 (2001)
10. Hollkamp, J.J., Gordon, R.W.: Reduced-order models for nonlinear response prediction: implicit condensation and expansion. J. Sound Vib. **318**(4), 1139–1153 (2008)
11. Lewandowski, R.: On beams membranes and plates vibration backbone curves in cases of internal resonance. Meccanica **31**(3), 323–346 (1996)
12. Touzé, C., Thomas, O., Chaigne, A.: Asymmetric non-linear forced vibrations of free-edge circular plates. Part 1: theory. J. Sound Vib. **258**(4), 649–676 (2002)
13. Amabili, M.: Nonlinear Vibrations and Stability of Shells and Plates. Cambridge University Press, Cambridge (2008)
14. Pierre, C., Jiang, D., Shaw, S.: Nonlinear normal modes and their application in structural dynamics. Math. Probl. Eng. **2006**, 1–15 (2006)
15. Touzé, C., Amabili, M.: Nonlinear normal modes for damped geometrically nonlinear systems: application to reduced-order modelling of harmonically forced structures. J. Sound Vib. **298**(4), 958–981 (2006)
16. Kerschen, G., Peeters, M., Golinval, J.-C., Vakakis, A.F.: Nonlinear normal modes, Part I: a useful framework for the structural dynamicist. Mech. Syst. Signal Process. **23**(1), 170–194 (2009)
17. Liu, X., Cammarano, A., Wagg, D.J., Neild, S.A.: A study of the modal interaction amongst three nonlinear normal modes using a backbone curve approach. In: Nonlinear Dynamics, vol. 1, pp. 131–139. Springer, Berlin (2016)
18. Liu, X., Cammarano, A., Wagg, D.J., Neild, S.A., Barthorpe, R.J.: Nonlinear modal interaction analysis for a three degree-of-freedom system with cubic nonlinearities. In: Nonlinear Dynamics, vol. 1, pp. 123–131. Springer, Berlin (2016)
19. Liu, X., Cammarano, A., Wagg, D.J., Neild, S.A., Barthorpe, R.J.: N-1 modal interactions of a three-degree-of-freedom system with cubic elastic nonlinearities. Nonlinear Dyn. **83**(1–2), 497–511 (2016)

http://www.springer.com/978-3-319-54403-8

Nonlinear Dynamics, Volume 1
Proceedings of the 35th IMAC, A Conference and Exposition on Structural Dynamics 2017
Kerschen, G. (Ed.)
2017, VIII, 221 p. 180 illus., 147 illus. in color.,
Hardcover
ISBN: 978-3-319-54403-8